The Astrophysical Journal, 954:77 (16pp), 2023 September 1 https://doi.org/10.3847/1538-4357/ace90e

Beyond BPT: A New Multidimensional Diagnostic Diagram for Classifying Power Sources Tested Using the SAMI Galaxy Survey

Victor D. Johnston[1], Anne M. Medling[1,2,10], Brent Groves[3], Lisa J. Kewley[2,4], Luca Cortese[2,3], Scott Croom[2,5], Ángel R. López-Sánchez[2,6,7,8], Henry Zovaro[2,9], Joss Bland-Hawthorn[5], Julia Bryant[5], Jon Lawrence[6], Matt Owers[6], Samuel Richards[5], and Jesse van de Sande[2,5]

[1] Ritter Astrophysical Research Center and Department of Physics & Astronomy, University of Toledo, Toledo, OH 43606, USA
[2] ARC Centre of Excellence for All Sky Astrophysics in 3 Dimensions (ASTRO 3D), Australia
[3] International Centre for Radio Astronomy Research, The University of Western Australia, 35 Stirling Highway, Crawley, WA 6009, Australia
[4] Center for Astrophysics | Harvard & Smithsonian, 60 Garden Street, Cambridge, MA 02138, USA
[5] Sydney Institute for Astronomy, School of Physics, A28, The University of Sydney, NSW 2006, Australia
[6] Department of Physics and Astronomy, Macquarie University, NSW 2109, Australia
[7] School of Mathematics and Physical Sciences, Macquarie University, NSW 2109, Australia
[8] Macquarie University Research Centre for Astronomy, Astrophysics & Astrophotonics, Sydney, NSW 2109, Australia
[9] Research School of Astronomy & Astrophysics, Mount Stromlo Observatory, Australia National University, Cotter Road, Weston, ACT 2611, Australia
Received 2022 November 30; revised 2023 July 2; accepted 2023 July 19; published 2023 August 25

Abstract

Current methods of identifying the ionizing source of nebular emission in galaxies are well defined for the era of single-fiber spectroscopy, but still struggle to differentiate the complex and overlapping ionization sources in some galaxies. With the advent of integral field spectroscopy, the limits of these previous classification schemes are more apparent. We propose a new method for distinguishing the ionizing source in resolved galaxy spectra by use of a multidimensional diagnostic diagram that compares emission-line ratios with velocity dispersion on a spaxel-by-spaxel basis within a galaxy. This new method is tested using the Sydney-Australian-Astronomical-Observatory Multi-object Integral-Field Spectrograph Galaxy Survey (SAMI) Data Release 3 (DR3), which contains 3068 galaxies at $z < 0.12$. Our results are released as ionization maps available alongside the SAMI DR3 public data. Our method accounts for a more diverse range of ionization sources than the standard suite of emission-line diagnostics; we find 1433 galaxies with a significant contribution from non-star-forming ionization using our improved method as compared to 316 galaxies identified using only emission-line ratio diagnostics. Within these galaxies, we further identify 886 galaxies hosting unique signatures inconsistent with standard ionization by H II regions, active galactic nuclei, or shocks. These galaxies span a wide range of masses and morphological types and comprise a sizable portion of the galaxies used in our sample. With our revised method, we show that emission-line diagnostics alone do not adequately differentiate the multiple ways to ionize gas within a galaxy.

Unified Astronomy Thesaurus concepts: Warm ionized medium (1788); Classification systems (253); Galaxy classification systems (582); Active galactic nuclei (16); Shocks (2086); Star formation (1569)

Supporting material: interactive figures

1. Introduction

Investigating the prevalence and effects of different ionizing sources within galaxies is a topic that has been of interest for decades (see Kewley et al. 2019, for a review). Separating different ionization mechanisms from one another in large extragalactic surveys has been primarily by use of optical diagnostic diagrams. These diagnostics compare key spectral features that are largely distinct for each ionizing source. For example, regions of high star formation ionize the surrounding H II regions with the radiation released from O and B stars. Active galactic nuclei (AGNs) emit a hard X-ray radiation field that is also capable of exciting nearby gas, to higher energy levels than star formation can. Supernovae and galactic winds can shock-heat gas, collisionally ionizing it.

The most prevalent optical emission-line diagnostic diagrams are the BPT (Baldwin et al. 1981) and VO87 (Veilleux & Osterbrock 1987) diagrams, which compare the flux ratios of emission-line pairs log([O III] λ5007/Hβ) and log([O I] λ6300/Hα), log([N II] λ6583/Hα), and log([S II] $\lambda\lambda$6716, 6731/Hα), and the WHAN diagram (Cid Fernandes et al. 2011) that compares the log([N II] λ6583/Hα) ratio to the equivalent width of Hα. These diagrams have proven useful because the different nature of each ionization source leads to different physical conditions in the ionized gas. The hard radiation field from an AGN produces higher ionization states in the surrounding interstellar medium as well as higher temperatures, increasing the strength of collisionally excited lines such as [O III] relative to the recombination lines like Hβ. Shocks have similarly elevated emission in the forbidden lines due to high temperatures, but also have extended zones of hot, partially ionized gas that lead to different flux ratios than AGNs (Veilleux & Osterbrock 1987).

These classification schemes were refined and popularized using single-fiber nuclear spectra from the Sloan Digital Sky Survey (SDSS; Adelman-McCarthy et al. 2006), showing that the central excitation source varies across the population of

[10] Hubble Fellow.

local galaxies. Star-formation-dominated galaxies have a metallicity-dependent track that lies below the maximum theoretical starburst line, while AGNs or shock-dominated galaxies are shifted upward due to the increased ionization parameter (Kewley et al. 2001, 2006, 2019; Kauffmann et al. 2003; Groves et al. 2006; Allen et al. 2008; Medling et al. 2015; Rich et al. 2015; Sánchez et al. 2015).

In addition to the use of emission-line diagnostics, kinematic information can be used to help identify ionization sources within a galaxy. It is well documented that shocks, due to the turbulent nature of collisions, have an increased velocity dispersion that correlates to the strength of the shock as compared to the relatively lower velocity dispersion of nearby star-formation-dominated regions (Monreal-Ibero et al. 2006, 2010; Rich et al. 2011, 2014; Law et al. 2021). These mechanisms have proved useful in identifying gas entrained within and ionized by outflows (López-Cobá et al. 2019, 2020; Law et al. 2021, 2022). Location within a galaxy, such as galactocentric radius, provides another useful check for yielding information on ionization sources. AGN ionization tends to occur closer to the nuclear region of a galaxy, while shocks are often associated with outflows and galaxy collisions (Sharp & Bland-Hawthorn 2010; D'Agostino et al. 2018; Sánchez et al. 2018; Lacerda et al. 2020).

Integral field spectroscopy (IFS) has enabled studies that compare these physical mechanisms across different spatial locations in a single galaxy (e.g., Sharp & Bland-Hawthorn 2010; Rich et al. 2011, 2014, 2015; Davies et al. 2014a, 2014b; Ho et al. 2014; Husemann et al. 2014; McElroy et al. 2015; Rodríguez del Pino et al. 2019). In order to gain a better understanding of the physical mechanisms that drive galaxy evolution, we require detailed information about not only what is happening inside them, but where as well.

In the past two decades, different IFS surveys have provided a wealth of simultaneous spatial and spectral information about galaxies. The Calar Alto Legacy Integral Field Area Survey has nearly 700 galaxy observations, with a subset focused on rarer galaxy types such as dwarf galaxies and low- and high-mass early-type galaxies (Sánchez et al. 2016). The Mapping Nearby Galaxies at APO Survey is an extension of SDSS that has observed roughly 10,000 galaxies of all sizes and types (Wake et al. 2017; Abdurro'uf et al. 2022). The Sydney-Australian-Astronomical-Observatory Multi-object Integral-Field Spectrograph Galaxy Survey (SAMI) contains over 3000 galaxies with a wide range of masses and morphological types in the nearby Universe (Croom et al. 2021). These surveys, and others of their kind, provide the required depth of data to investigate ionizing sources on large scales that were previously impossible.

A recent example of the power of IFS data, in particular their ability to help identify ionization sources, can be seen in the work of D'Agostino et al. (2019). Created using data on NGC 1068 taken from the Siding Spring Southern Seyfert Spectroscopic Snapshot Survey (Thomas et al. 2017), these authors shows how spatially resolved emission-line fluxes, as well as derived gas kinematics and physical radius, can be used to separate regions of pure star formation, AGNs, and shock ionization from one another. This technique uses a combination of several methods discussed above in order to reduce the amount of degeneracy that any one individual method has in determining ionization sources. Indeed these basic principles form the basis of our work presented below.

In this paper, we demonstrate a new automated classification method that uses a combination of emission lines and kinematics to separate star formation, AGNs, and shocks on a spatially resolved scale. We also identify a number of populations that are distinct from the standard interpretation of star-forming galaxies being dominated by young stellar emission. Section 2 describes the data used from Data Release 3 (DR3) of the SAMI Galaxy Survey. Section 3 reviews the limitations of existing emission-line diagnostic methods. Section 4 contains the methods and implementations of the new classification scheme. Section 5 compares the results of our new schema to the classical emission-line diagnostics and explains the advantages of using additional kinematic and spatial information. Finally, Section 6 contains an overview of the shock map data products that we are releasing and Section 7 presents our conclusions.

2. The SAMI Galaxy Survey

We use optical IFS collected from the SAMI Galaxy Survey on the 3.9 m Anglo-Australian Telescope at Siding Spring Observatory (Croom et al. 2012). The SAMI instrument observes each target with a fiber bundle consisting of 61 fibers, allowing for a field of view (FOV) of 15″ per observation (Bland-Hawthorn et al. 2011; Bryant et al. 2014). The SAMI Galaxy Survey Data Release 3 contains 3068 galaxies (Croom et al. 2021) and spans a wide mass range from $\log(M_\star/M_\odot)$ of 7.5–11.6 and a range in redshift of $0.004 < z < 0.113$ (Scott et al. 2018). The galaxies observed with SAMI were chosen from the Galaxy and Mass Assembly (GAMA) Survey (Driver et al. 2011). The SAMI instrument is composed of a blue arm and a red arm that span the majority of the visible wavelength range. For the SAMI Galaxy survey we use the 580V grating at 3750–5750 Å, giving a resolution of $R = 1808$ ($\sigma = 70.4$ km s^{-1}), and the R1000 grating from 6300–7400 Å, giving a resolution of $R = 4304$ ($\sigma = 29.6$ km s^{-1}; van de Sande et al. 2017; Scott et al. 2018). The resulting spatial scale of the data cube is 0.″5 per pixel with a 50×50 image for a total FOV of $25'' \times 25''$. Galaxies from a wide range of environments were collected, from isolated field galaxies to large groups and clusters (Bryant et al. 2015; Owers et al. 2017).

The emission-line fitting was performed using the LZIFU software package (Ho et al. 2016; Medling et al. 2018). Each spectrum is fit with the following 11 strong lines simultaneously: Hα, Hβ, [O III] $\lambda\lambda$4959, 5007, [O I] λ6300, [N II] $\lambda\lambda$6548, 6583, [S II] $\lambda\lambda$6716, 6731, and [O II] $\lambda\lambda$3726, 3729, with up to three Gaussian components for each, and merged using the trained neural net LZCOMP (Hampton et al. 2017). All ionized gas species are constrained to have the same kinematic profiles. Multiple components are fit in order to account for the kinematically distinct phases of the ionized gas, such as outflowing material, allowing for a more accurate representation of emission from the gas. The resulting data products are two-dimensional spatial maps where emission-line flux, velocity, and velocity dispersion are extracted. For our diagnostics we adopt a minimum signal-to-noise ratio of 3 for each emission line used in our analysis. We also only include galaxies that have 10 or more spaxels remaining after this cut. This cut ensures that the results of our analysis are not skewed by faint, low-signal galaxies. We also calculate a projected galactocentric radius of each spaxel by using the redshift and

inclination data provided in the SAMI catalogs for each galaxy (Bryant et al. 2015; Owers et al. 2017).

3. Breaking the Shock Degeneracies

The spatially resolved nature of IFS has proven useful in identifying trends relating to the ionization structure of galaxies. Excitation from AGNs tends to be found toward the central region of a galaxy, though it is possible that the hard ionizing field can dominate further out into the galaxy (Hainline et al. 2014). Shocked gas, however, can be linked to many different physical processes and is therefore not expected to be contained in any particular region of a galaxy. When multiple excitation sources are present within a galaxy, their spatially resolved emission-line diagnostic diagrams produce mixing sequences, showing the progression from the star-forming region into the AGN and LINER regions of the emission-line diagnostics as the relative fraction of ionization from AGNs or shocks increases (Davies et al. 2014a, 2014b).

Shocked gas is not well separated by the BPT/VO87 diagnostic diagrams, because its line ratios are degenerate with those of AGNs (Allen et al. 2008; Thomas et al. 2016). Because of this overlap in emission-line space, it is impossible to separate them without additional information. One such way to differentiate shocks from other excitation sources is to look at the kinematics to see how turbulent regions of a galaxy are. Given that shock excitation is a mechanical process rather than radiative, shocked gas tends to be more kinematically disturbed. It has been shown that gas ionized by stars (or gas within H II regions) has significantly lower velocity dispersions, typically less than 50 km s^{-1}, than shocked gas, which has 100 km s^{-1} or higher (Rich et al. 2011, 2015; Davies et al. 2014a).

An additional challenge in characterizing gas excitation sources is that it is difficult to examine a large number of galaxies at once. The combination of line ratios, kinematics, and spatial information has so far proved to be the most reliable method of determining the power sources of galactic outflows. A way to quickly classify outflows while keeping the multiple dimensions of information was proposed by D'Agostino et al. (2019) in a new 3D diagnostic diagram. This diagram uses velocity dispersion, projected radius, and a modified line ratio to determine two distinct tracks from star formation to shock and AGN excitation. Tested on an actively star-forming galaxy that has a known AGN and shows shock activity, this method provides a great example of the new level of analysis that is possible with IFS. Because shocks and AGNs lie in separate regions in this diagram, it is possible to determine the separate mixing sequences of both. This allows for a fractional contribution of each power source to be determined at each spatial location. The degeneracies that were present on the BPT/VO87 diagrams are resolved here.

Though this method easily breaks the degeneracies in the extreme case of NGC 1068, it does not separate AGN-ionized and shock-ionized gas in the more moderate SAMI sample. This degeneracy is likely due to several reasons, the most prominent being that due to the closeness of NGC 1068, the spatial resolution of the data ($\sim$100 pc px^{-1}) is at a much smaller physical scale than that of a typical SAMI galaxy (median of 1.65 kpc px^{-1}). This drastic improvement in spatial resolution allows better separation between the multiple sources of ionization found within a galaxy that would otherwise be blended together on larger scales. This blending prevents their classification scheme from being broadly applicable to data from surveys with spatial resolutions worse than $\sim$1 kpc px^{-1}. We are therefore motivated to extend the 3D diagnostic diagram technique to find one sensitive enough to classify SAMI galaxies, and other current large IFS surveys, that works on both small and moderate spatial scales.

4. New 3D Classification Scheme

We propose a new classification method using a combination of emission-line ratios and kinematics for determining the main excitation source of warm ionized gas. Our new diagnostic uses the same emission-line ratios as the standard BPT/VO87 diagrams, while adding a third axis of velocity dispersion to further investigate the physical nature of the gas. By using this combination of parameters, we are able to detect fainter signatures of shocks and AGNs than with any other method. We also detect multiple populations of galaxies whose classifications from their emission-line ratios are inconsistent with the physical interpretation given by their velocity dispersion. We do this by identifying and tracing the mixing sequence from star-forming gas to either a shock track or an AGN track. By following these mixing sequences we can extract the relative shock or AGN fraction for an individual spaxel within a galaxy on a per-galaxy basis.

The first step in our new method involves identifying galaxies that have signatures of AGN-like ionization in all three of the BPT/VO87 diagrams. We use a criterion of requiring 10 spaxels in each of the AGN regions and do not use any velocity dispersion cutoffs for this group. This is to ensure that galaxies that are being ionized primarily by the hard radiation field of the black hole with no shock component are not misclassified because they lack any elevated velocity dispersion. We use the equivalent width of the emission of Hα as an additional parameter to further separate AGN ionization from contamination from regions of hot low-mass evolved stars (HOLMES). If 70% of the AGN-like spaxels have an equivalent width of 3 Å or less, the galaxy is classified as being dominated by HOLMES emission, otherwise it is considered a true AGN.

We next examine the distribution of velocity dispersions for signatures of multiple kinematic components in each galaxy individually. For this we use the multiple component spectral fits provided by LZIFU. We then use a multicomponent Gaussian fit to the histogram of the velocity dispersion to see whether there is a population of gas that is distinct from the standard, low-velocity-dispersion star-forming regions. If the range of velocity dispersion is best fit with two components, or if the peak of the single component minus one standard deviation is greater than 50 km s^{-1}, the gas is flagged as kinematically disturbed. Both the kinematically disturbed gas and the nonkinematically disturbed gas are then examined using their emission-line ratios.

Starting with the kinematically disturbed galaxies, we see where the spaxels lie on the classical BPT/VO87 diagrams. To be considered as containing a significant contribution from an ionization source, we require 10 spaxels or more in a given region for two out of three of the log([N II]/Hα), log([S II]/Hα), and log([O I]/Hα) diagnostics. This leads to four cases: AGN-like, LINER-like, AGN- and LINER-like, and star-forming-like ionization. For AGN-like ionization we again check the equivalent width of Hα to separate out HOLMES contamination. If no significant HOLMES contribution is found the galaxy is classified as an AGN, otherwise it is moved

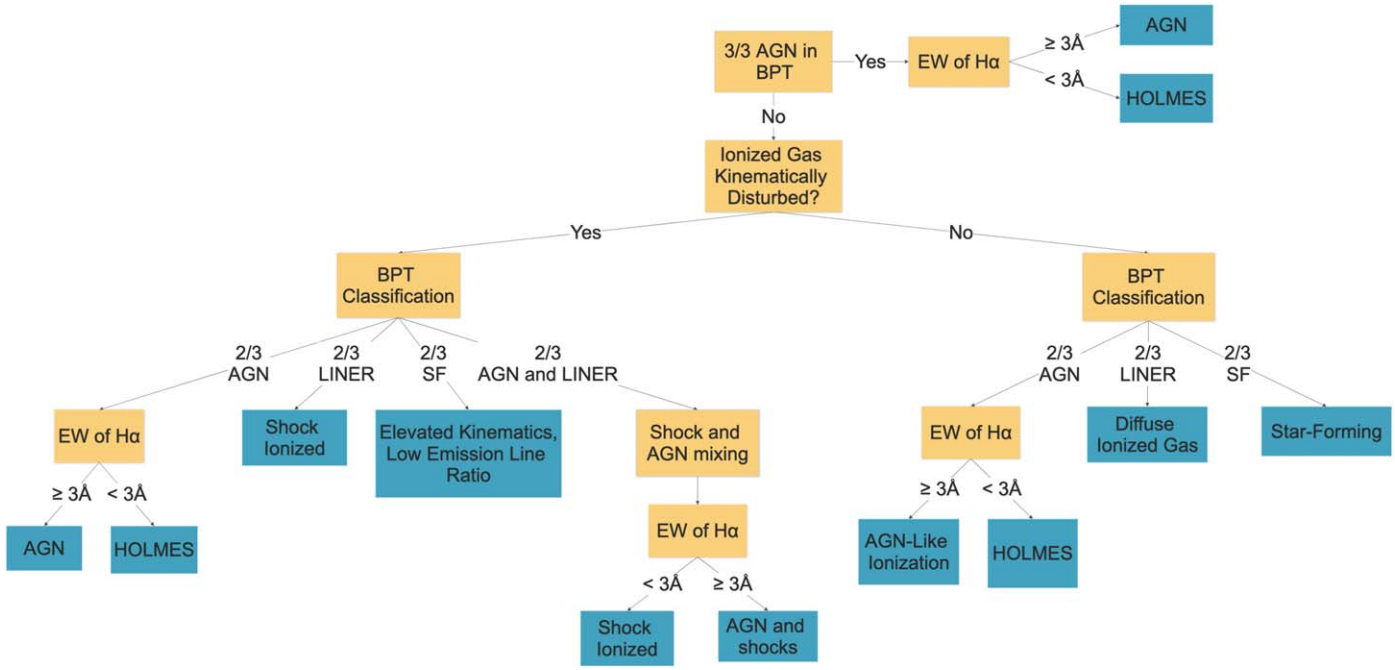

Figure 1. A flowchart showing a simplified decision tree used by our classification method. The yellow boxes show steps in the classification process while the other colored boxes represent the final classification that a galaxy can fall into.

to the HOLMES category. We use this criterion of two out of three emission lines plus velocity dispersion for these AGNs as these galaxies are likely ones that host AGNs with mild outflows. For the LINER-like galaxies, we classify all of these as being shock-ionized because the emission-line ratios and their high velocity dispersion match the classic case of turbulent, collisionally excited gas. Galaxies with AGN- and LINER-like ionization are checked once again for HOLMES contamination, and are labeled as shock-ionized if the AGN-like spaxels are contaminated with HOLMES, and as AGNs if they are not. For these galaxies with AGN- and LINER-like ionization not contaminated by HOLMES, we label them as AGNs even though they show significant signatures of shock excitation because they are most likely galaxies that host strong outflows from the central AGN region. Finally, for galaxies that do not contain significant signatures of non-star-forming-like ionization, we label them as their own category of elevated velocity dispersion with low emission-line ratio. As their velocity dispersions are not consistent with pure H II ionization, we are hesitant to classify all of these galaxies as simply star-forming. A further discussion of this group is located in Section 5.6.

Now we look at the galaxies with no elevated velocity dispersion. Again, we use a criterion of two out of three regions of the emission-line diagnostics as explained above. This presents three cases instead of four this time: AGN-like, LINER-like, and star-forming-like. For AGN-like galaxies we perform the same HOLMES check as in the other AGN-like cases and label those without HOLMES contamination as simply hosting AGN-like ionization. It is worth explicitly stating that we do not label these galaxies as containing true AGNs, but only as hosting AGN-like ionization. Our reasoning for this is explained in Section 5.5. For LINER-like galaxies, we classify them as hosting ionization from diffuse ionized gas as their low velocity dispersions are inconsistent with shock-ionized gas. The remainder of the galaxies are classified as classical star-forming galaxies as they have both low velocity dispersions and low emission-line ratios.

A flowchart showing an overview of the classification scheme is shown in Figure 1 for quick reference, and an in-depth breakdown of each category can be found in Section 5.

We describe two examples of a galaxy hosing either shock or AGN ionization here, for GAMA galaxies 106717 and 376478 respectively. Figure 2 shows the BPT/VO87 diagnostics as well as a spatial map for each diagram for GAMA 106717, which contains regions of shocked gas. It is clear that this galaxy hosts LINER ionization that is spatially consistent between multiple pairs of emission-line ratios. Figure 3 shows the results of our new classification scheme. The first row is the BPT/VO87 diagrams with spaxels marked according to our new method: black points have only star-forming ionization and the colored points are the spaxels with high velocity dispersion colored according to increasing radius, which for GAMA 106717 correspond to spaxels that contain shock ionization. The middle row is velocity dispersion versus log ([N II]/Hα), log([O III]/Hβ), and projected galactocentric radius colored the same as the plots above. From the projections in velocity dispersion space, two distinct populations of gas can be seen that start at low velocity dispersion and increase with emission-line ratios. Two mixing sequences can be drawn from these plots, one for the low-velocity-dispersion star-forming gas and another for the high-velocity-dispersion shocked gas, which both begin at a single point at the base of the star-forming sequence in the log([N II]/Hα) diagram. The last row contains a histogram and a map of the velocity dispersion, a map of the shock fraction, which is described in more detail in Section 6, and an optical image of the galaxy for reference. The combination of kinematic information and emission lines is what allows us to detect faint signatures of shock ionization in this galaxy that would be missed with emission-line ratios alone.

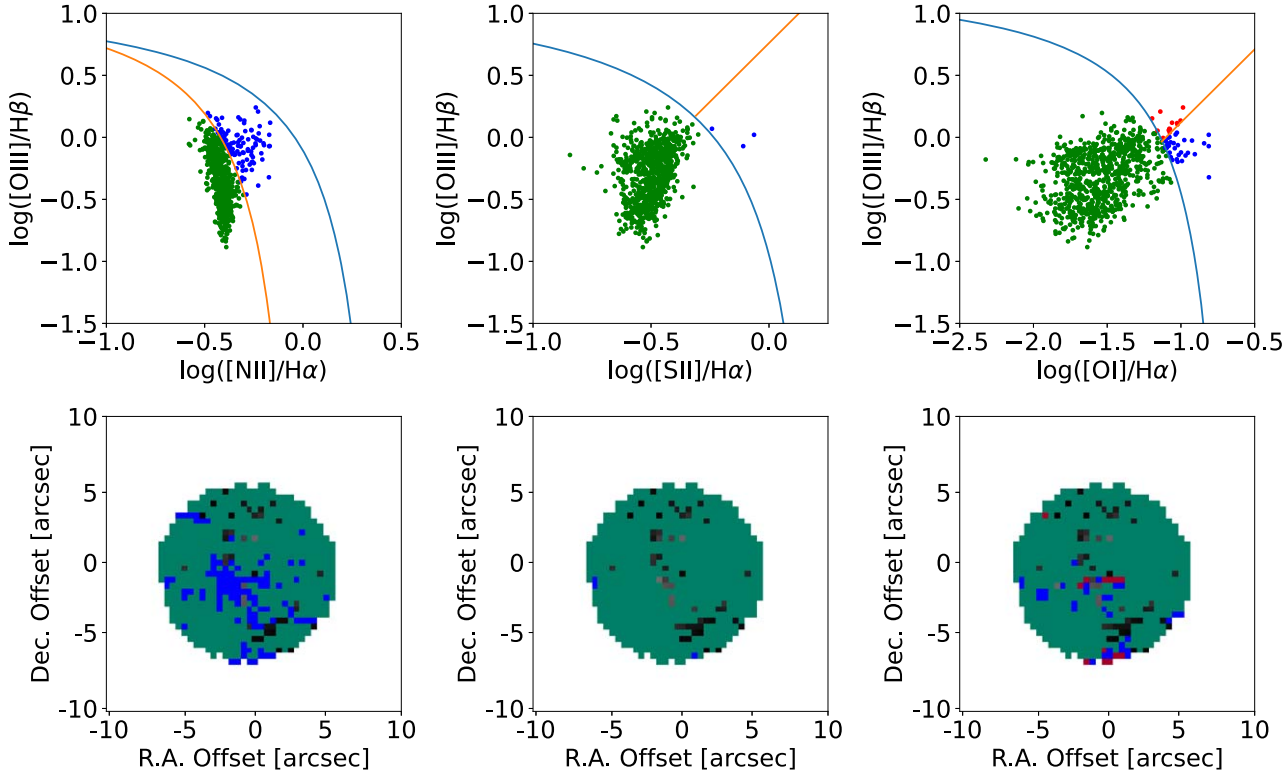

Figure 2. Emission-line diagnostics and spatial maps for GAMA 106717. Each figure in the first row shows the emission-line diagnostics colored according to where each spaxel falls in its respective diagram: green for star-forming, blue for composite or LINER, and red for AGN. Below each diagnostic is the corresponding spatial map showing where in the galaxy the points in the diagram above are located.

Figures 4 and 5 show similar results to Figures 2 and 3, but for GAMA 376478, which contains AGN excitation. Clear signatures of AGN ionization can be seen in the emission-line diagnostics and spatial maps in Figure 4, but more spaxels are detected that are traced further away from the nucleus of the galaxy with our revised method.

While our new diagnostic was tested with the data from the SAMI Galaxy Survey, the methods used are general enough to apply to any IFS data. As long as the spectral resolution is able to resolve roughly 30 km s^{-1} in velocity dispersion to separate the non-star-forming gas from the excited regions, the proposed method is viable. An increase in spatial resolution also helps to further separate the mixing sequences from one another, as shown in D'Agostino et al. (2019).

5. Comparison with Standard Diagnostics

Here we compare the results of our new classification scheme with those that use the classical BPT/VO87 diagrams without the additional use of kinematic or equivalent width information. For this work, we label a galaxy as star-forming, AGN, or shocked in emission-line space only if there are a minimum of 10 spaxels or more in each of the three BPT/VO87 diagrams in their respective regions after applying the same cutoff in signal-to-noise ratio as our revised method. This strict criterion ensures that we are not including low-signal galaxies that could inflate the numbers of AGNs and shocked regions. Of the 3068 galaxies in the SAMI sample, 1996 of them remain after the cut in signal-to-noise ratio. From this remaining sample, using only BPT/VO87 diagnostics, we find that 233 galaxies contain clear signs of shocked gas, 50 host signatures of AGN ionization, and 33 show signatures of both shock and AGN ionization simultaneously. The remaining 1680 galaxies are identified as primarily hosting only ionization associated with H II regions or star formation.

For comparison, our new classification scheme detects 409 galaxies containing signatures of pure shock ionization, 68 containing only AGN ionization signatures, 70 galaxies containing shock and AGN signatures, 173 HOLMES-contaminated galaxies, 105 galaxies with diffuse ionized gas signatures, 251 galaxies with AGN-like ionization, 563 pure star-forming galaxies, and 357 galaxies with elevated velocity dispersion and low emission-line ratios. Figure 6 shows the results of our new classification scheme compared to BPT/VO87 emission-line diagnostics alone.

For galaxies identified as hosting kinematically disturbed AGNs or shocks, we also see an increase in the number of spaxels identified as being ionized by shocks or AGNs on a galaxy-by-galaxy basis due to being able to trace the mixing sequence further into the star-forming region of the emission-line diagnostic diagram. This can be most easily seen by comparing the classification by emission-line ratio only in Figures 2 and 4 with its new counterpart in the map of ionization fraction in Figures 3 and 5 respectively. We will discuss here in more depth each of the categories of classification.

5.1. Star-formation-dominated Galaxies

There are 563 galaxies identified as being dominated by ionization from H II regions with no signs of AGNs or shock excitation. These galaxies all have velocity dispersions of less than 50 km s^{-1}, which is consistent with star-formation-dominated regions (Rich et al. 2011, 2015; Davies et al. 2014a). The emission-line ratios of these galaxies also lie below the maximum theoretical starburst line, indicating a

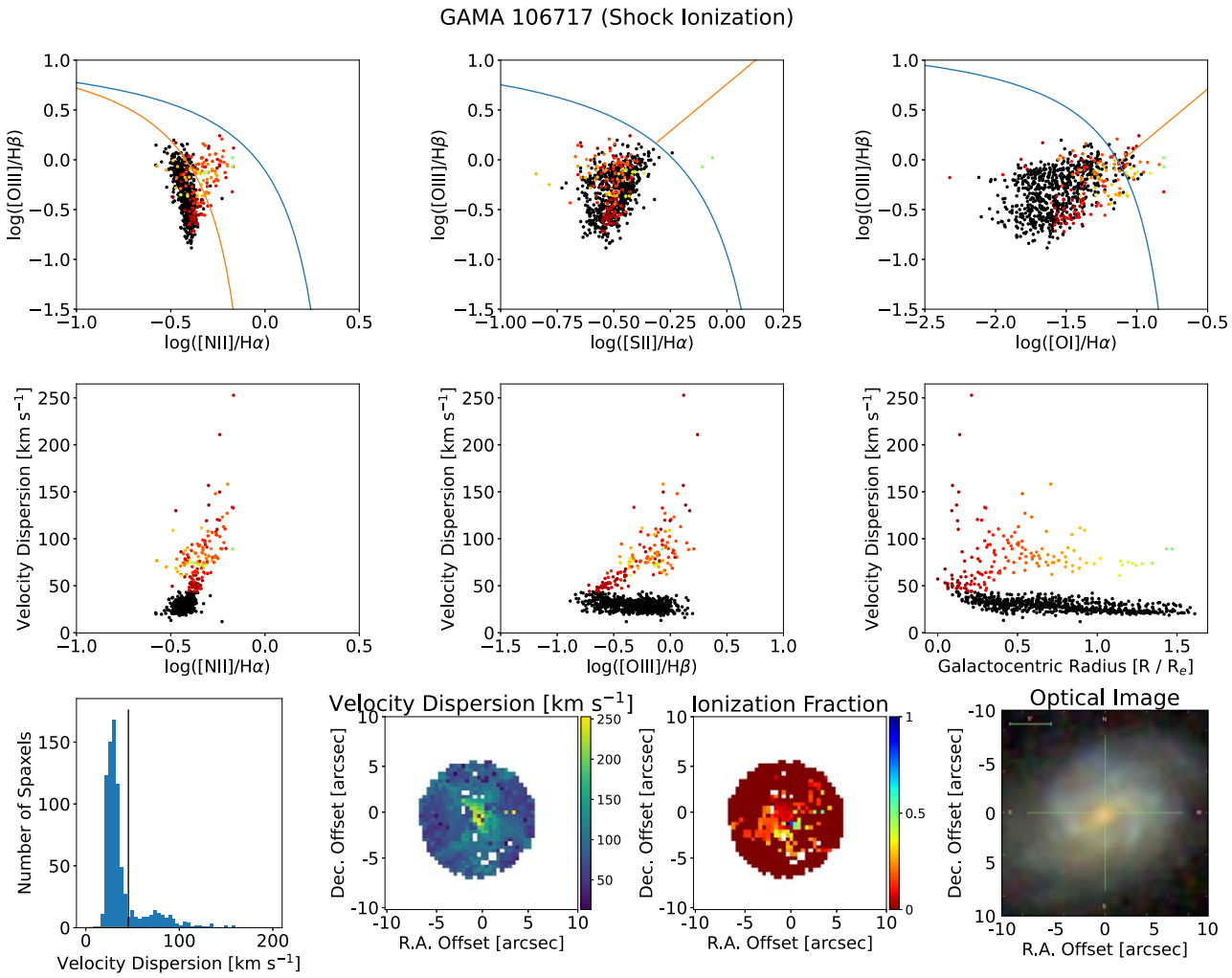

Figure 3. Emission-line diagnostics and maps for GAMA 106717. The first row are the BPT/VO87 diagrams colored according to our new diagnostic: black points are spaxels dominated by star formation and colored points are spaxels with shock ionization colored by increasing radius from the center of the galaxy. The middle row contains plots of log([N II]/Hα), log([O III]/Hβ), and effective radius vs. velocity dispersion. The separation between shocked and star-forming gas can be easily seen in the middle and right panels in this row. The last row contains a histogram of the velocity dispersion with a vertical line separating the groups of gas with low and high velocity dispersion, a map of the velocity dispersion, a map of shock fraction, which shows the relative contribution of shocks on a per-spaxel basis, and a three-color image on the right matching the FOV of the SAMI data.

weaker source of ionization than is typically found with AGNs or shocks. The combination of low velocity dispersions and low emission-line ratios strongly suggests that these galaxies lack any significant contribution to their ionization from either widespread shocks or AGNs, and are therefore classified as star formation dominated.

5.2. Shocked Galaxies

We identify 409 galaxies as hosting clear signatures of shock excitation, as opposed to 233 galaxies using emission-line diagnostics only. Each of these galaxies has an elevated velocity dispersion that is typical of turbulence caused by the mechanical nature of collisionally excited gas. These emission-line diagnostics correlate with LINER-like ionization. A mixing sequence can be drawn for each of these galaxies by tracing the kinematically disturbed gas from areas of low velocity dispersion and low emission-line ratio to higher values of each. This allows us to follow the shock excitation from the most extreme values down to the base of the star-forming sequence. Figure 3 shows an example of this mixing sequence in more detail. By using this mixing sequence, we often trace the shock excitation below the standard classification lines as the sequence moves from high to low shock contribution.

5.3. Separating HOLMES from AGNs

Here we explore a further step used to ensure the purity of our AGN classification. The presence of HOLMES can present itself as an increased emission-line ratio that mimics that of AGNs or shocks (Binette et al. 1994; Stasińska et al. 2008; Cid Fernandes et al. 2010a, 2010b). One reason for this is that an evolved stellar population that lacks young stars produces ionization that matches that of non-star-forming regions in emission-line diagnostics. These hot low-mass evolved stars can make a significant contribution to the ionization of a galaxy, especially in galaxies with a lack of young stars such as ellipticals and early-type spiral galaxies (Lacerda et al. 2018; Sánchez 2020; Sánchez et al. 2021). One way to account for this is to use the equivalent width of Hα as a tracer of these regions. Cid Fernandes et al. (2011) have shown that spectra in which HOLMES dominates tend to have $EW_{H\alpha} \leqslant 3$ Å.

To this end, we perform an additional check on all of the galaxies identified as containing AGN-like ionization in our

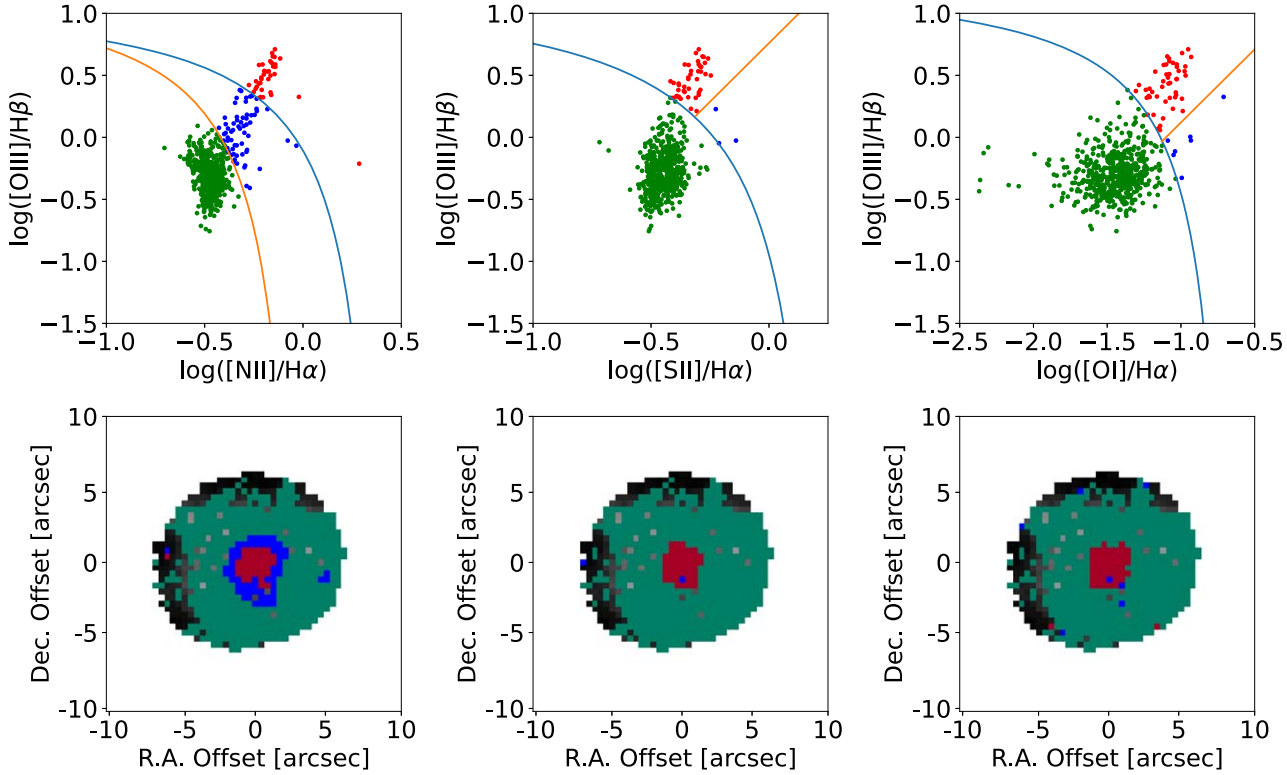

Figure 4. Emission-line diagnostics and spatial maps for GAMA 376478. Each figure in the first row shows the emission-line diagnostics colored according to where each spaxel falls in its respective diagram: green for star-forming, blue for composite or LINER, and red for AGN. Below each diagnostic is the corresponding spatial map showing where in the galaxy the points in the diagram above are located.

sample to investigate the contribution and possible contamination of HOLMES in these galaxies. When looking at the distribution of equivalent widths of Hα in our AGN sample before accounting for HOLMES, we can see a clear bimodal distribution with a separation between two populations at an $EW_{H\alpha}$ of 3 Å as shown in Figure 7. This distribution strongly suggests that a portion of our AGN galaxies show traces of HOLMES contamination at some level. Since it is possible that an AGN can present AGN-like $EW_{H\alpha}$ for the nuclear region before falling off to lower values radially, we do not apply a global cutoff to all spaxels of less than 3 Å. Instead, we look at the fraction of AGN-like spaxels that lie above and below the $EW_{H\alpha}$ cutoff on a per-galaxy basis. The selection criterion used here requires that 70% of a galaxy's spaxels that we identify as AGN-ionized must have an $EW_{H\alpha}$ of less than 3 Å before being reclassified as HOLMES. This is done so that galaxies with weak AGNs are not missed if only the central spaxels have a large $EW_{H\alpha}$ while spaxels further from the center have lower values. Of the 311 AGN-like galaxies initially identified with our schema, 173 of these galaxies contain 70% or more of their AGN spaxels showing HOLMES-like equivalent widths that we reclassify. This brings our total number of AGN galaxies to 138. This combination of emission-line ratios, gas kinematics, and $EW_{H\alpha}$ helps to ensure that the galaxies that we label as AGNs do indeed host a nonnegligible fraction of AGN ionization.

5.4. AGN-hosting Galaxies

After accounting for HOLMES ionization, our sample is left with a total of 138 AGN galaxies; 43 of these are identified from emission-line diagnostics alone, 70 show elevated velocity dispersions and signatures of AGN and LINER ionization, and 25 show elevated velocity dispersions and AGN signatures, but no significant LINER ionization. We provide these different avenues for classification due to the different physical natures of each of them. The 43 emission-line-only galaxies are selected without using any kinematic information because a purely radiative AGN without shocks or outflows can still cause extreme ionization without mixing up the surrounding gas. This process would present itself as an increased emission-line ratio while not necessarily having increased velocity dispersion. We require agreement in all three of the BPT/VO87 diagrams in order to classify a galaxy as hosting an AGN due to the fact that galaxies that only have AGN-like ionization in two out of three emission-line diagnostics look much different than those that have it in all three. We explore these two-out-of-three galaxies in more detail in Section 5.5.

The 95 AGNs selected with enhanced emission lines and velocity dispersions are likely indicative of AGNs with some form of gas flow. These galaxies have AGN-like emission while also having velocity dispersions not associated with pure star formation or a purely radiative AGN. 70 of these 95 galaxies also have significant amounts of LINER-like ionization detected as well, further supporting the possibility of shock-induced AGN outflows. While many of these galaxies would be classified as both shock- and AGN-ionized, we label them as AGNs in the final classification because it is likely that the shocks are being driven by the AGNs in the center of these galaxies.

5.5. AGN-like Galaxies

We denote a special category of AGN-like galaxies that are separate from standard AGNs. This category contains 251 galaxies and is characterized as having low velocity dispersions

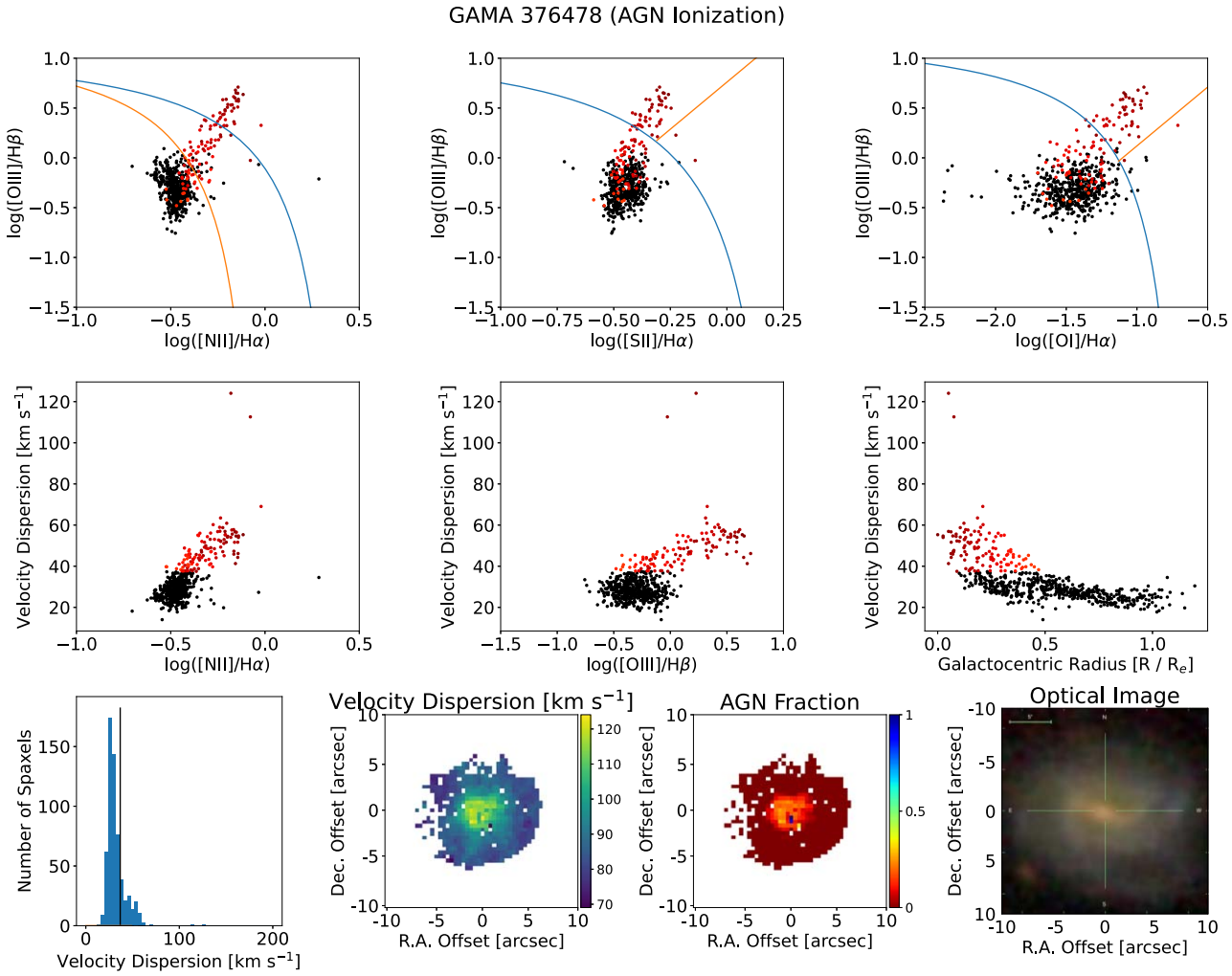

Figure 5. Emission-line diagnostics and maps for GAMA 376478. The first row are the BPT/VO87 diagrams colored according to our new diagnostic: black points are spaxels dominated by star formation and colored points are spaxels with AGN ionization colored by increasing radius from the center of the galaxy. The middle row contains plots of log([N II]/Hα), log([O III]/Hβ), and effective radius vs. velocity dispersion. The last row contains a histogram of the velocity dispersion with a vertical line denoting the two components in velocity dispersion space, a map of the velocity dispersion, a map of the AGN fraction, which shows the relative contribution of AGN ionization on a per-spaxel basis, and a three-color image on the right matching the FOV of the SAMI data.

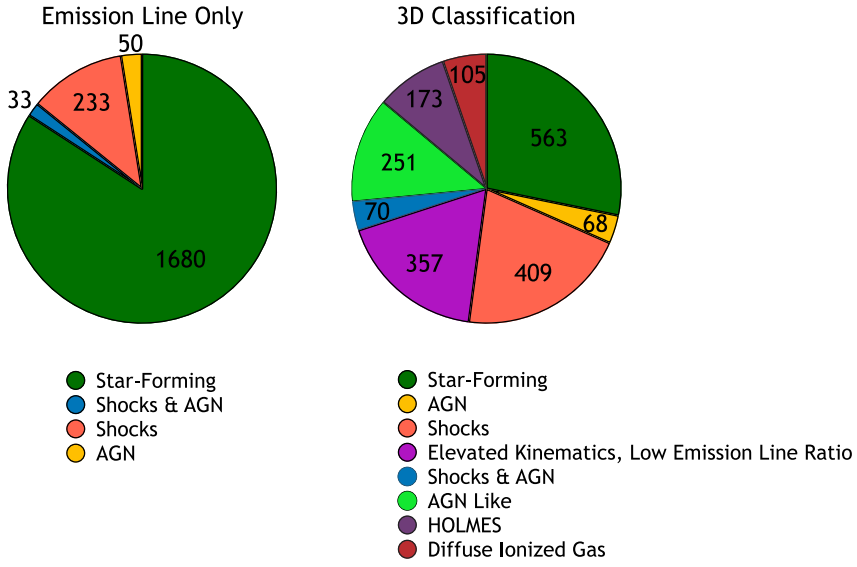

Figure 6. A comparison of ionization sources detected using just the BPT/VO87 diagrams (left) and our new method using emission-line ratios, kinematics, and spatial information (right). Our 3D classification method is more sensitive at detecting ionization from non-star-forming sources than just emission-line diagnostics alone.

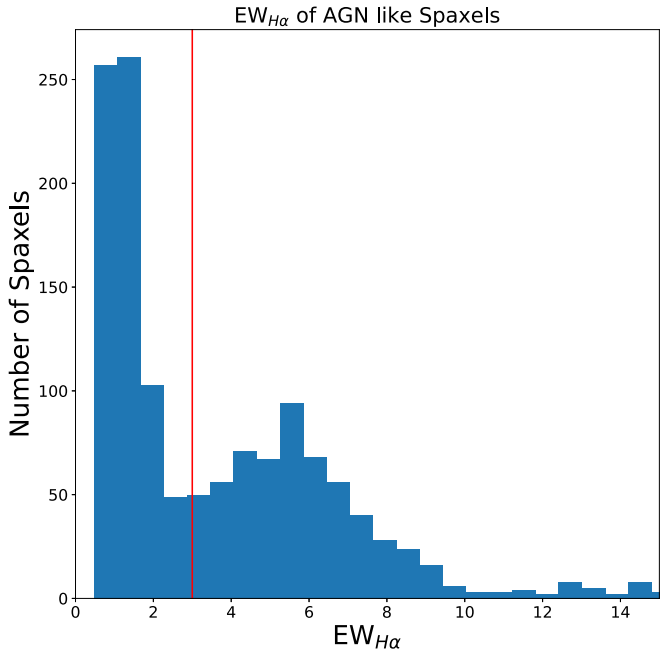

Figure 7. A histogram of the distribution of $EW_{H\alpha}$ for AGN-like spaxels. The red vertical line shows the 3 Å separation used to distinguish between HOLMES and true AGN ionization.

and exactly two out of three AGN-like emission-line diagnostics. They also are not contaminated by HOLMES, as those cases have been moved into the proper category already. These cases stand out as being unlike a typical AGN galaxy in that there is no spatial coherence between the AGN-like spaxels within a galaxy. The mass of these galaxies also tends to be much lower than that of the sample with elevated velocity dispersion or three out of three AGN-like diagnostics as shown in Figure 8. The morphological type is almost exclusively late spirals as well, with only 10 out of 251 galaxies not being a late spiral type. The location of spaxels on the emission-line diagnostics is also unique in that they tend to clump together toward the low-metallicity regions in the top left of each diagram, and extend nearly horizontally into the AGN region in the [S II] and [O I] diagrams, sometimes reaching into the LINER region as well. Figure 9 shows GAMA 273514, which contains this AGN-like ionization. There is no noticeable structure in the spatial map for any of the AGN-like spaxels, and the [N II] diagram does not show any AGN-like spaxels at all. Nearly all of the galaxies in this population follow the same emission-line diagnostic and spatial trends as GAMA 273514.

Despite the often large number of AGN-like spaxels in these galaxies, and given the combination of an on-average low galaxy mass, a single morphology type, no trace of any elevated velocity dispersion, and the lack of spatial structure in the emission-line maps, we do not classify these galaxies as true AGN hosts but rather as hosting AGN-like emission. While it is certainly possible that a number of these galaxies do indeed host an AGN, to determine whether they are true AGN hosts would require a more in-depth look at each galaxy individually, which is beyond the scope of this survey-wide study.

5.6. Elevated Velocity Dispersion, Low Ionization

There are 357 galaxies we identify that have elevated velocity dispersion but few or no spaxels with high enough emission-line ratios to be identified as shocks or AGNs on their own. By using the kinematics, we can still identify a mixing sequence separate from the star-forming sequence, but are unable to trace it beyond the star-forming regions of BPT/VO87 line ratio space to identify whether the secondary ionization process is shocks or AGNs. It is possible that a number of these galaxies are the result of beam-smearing artificially increasing the velocity dispersion. Because of the difficulty in separating the effects of beam-smearing from real, physical processes within the galaxies for these cases, we label them simply as elevated velocity dispersion, low ionization and leave the final classification to the user based on their science goals. Figure 10 shows an example of one of these galaxies.

5.7. Diffuse Ionized Gas

A number of galaxies were found that have LINER-like ionization in emission-line ratio diagnostics, but low velocity dispersions associated with pure star formation. These galaxies are interesting in that while they have enough spaxels to be classified as non-star-forming in emission-line space, they do not have kinematic signatures associated with shocks. These galaxies all share a similar trend of having regions of gas that extend into the LINER space in at least two of the BPT/VO87 diagrams while having velocity dispersions of $<50\,\mathrm{km\,s^{-1}}$ for the entire galaxy. The majority of their spaxels tend to lie along the maximum theoretical starburst line and do not typically extend much into higher emission-line space. Their velocity dispersion profiles are all consistent with purely star-forming gas and show no signs of having two distinct tracks. Figure 11 shows GAMA 298666, an example of a galaxy hosting LINER-like ioniziation with low velocity dispersion. Due to the velocity dispersion being inconsistent with shocks, we label this galaxy as hosting ionization from diffuse ionized gas.

For the 105 galaxies with LINER-like ionization and low velocity dispersions, one possible explanation is that they contain diffuse ionized gas, which would have elevated line ratios while having a lower velocity dispersion (Reynolds et al. 1973; Belfiore et al. 2022; Micheva et al. 2022). Traditionally, diffuse ionized gas is primarily detected in edge-on spiral galaxies at low redshifts (Dove & Shull 1994; Miller & Veilleux 2003). The nature of diffuse ionized gas would align with the spread-out nature of the elevated emission-line ratios with low velocity dispersion. These elevated emission-line ratios could also be caused by ionization from post-asymptotic giant branch stars. The radiation released from these stars can ionize the surrounding medium without mixing up the gas (Binette et al. 1994; Stasińska et al. 2008; Cid Fernandes et al. 2011). Future in-depth analysis of these galaxies is needed to confirm the physical processes at play; here we simply classify them as diffuse ionized gas.

6. Ionization Maps

As part of our analysis we have created ionization map data products that show the fractional contribution of each possible ionization source on a per-spaxel basis for those galaxies that have elevated velocity dispersions. These values are calculated separately for each galaxy and are not global. The data products are image files consisting of three layers: star formation, AGN, and shock contribution. Each layer shows the spatial map of the fractional contribution to the emission-line fluxes by each ionization source. As we are unable to separate both AGNs and

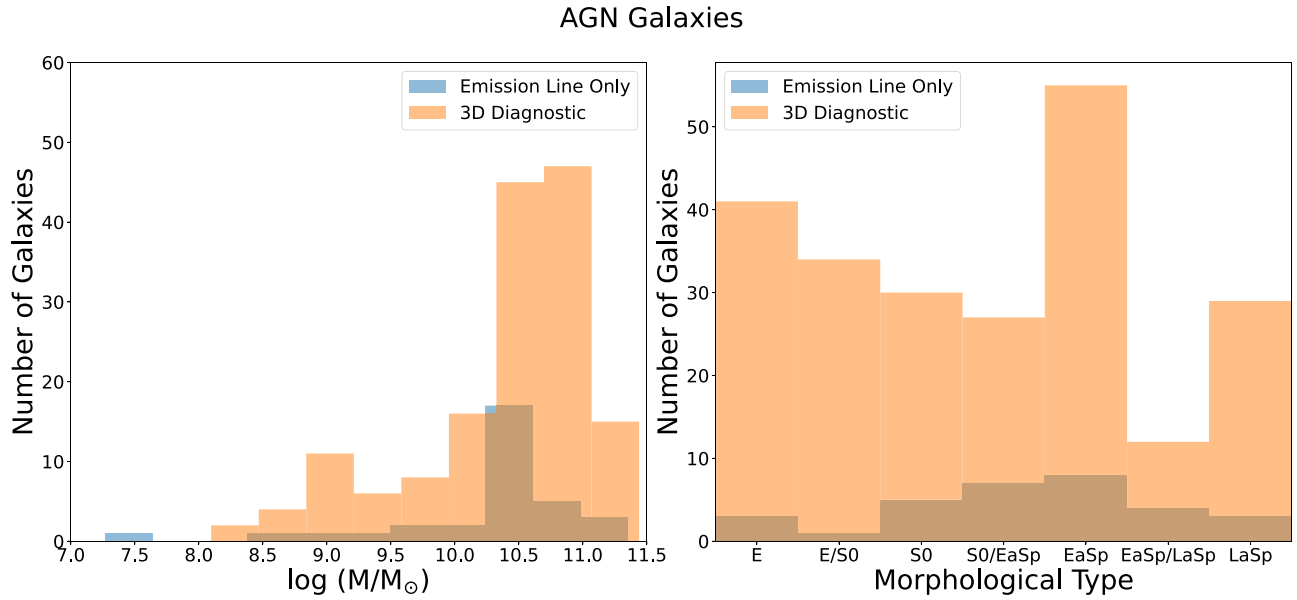

Figure 8. Histograms showing the distribution of galaxy mass and morphological type for galaxies identified as hosting AGNs and AGN-like ionization.

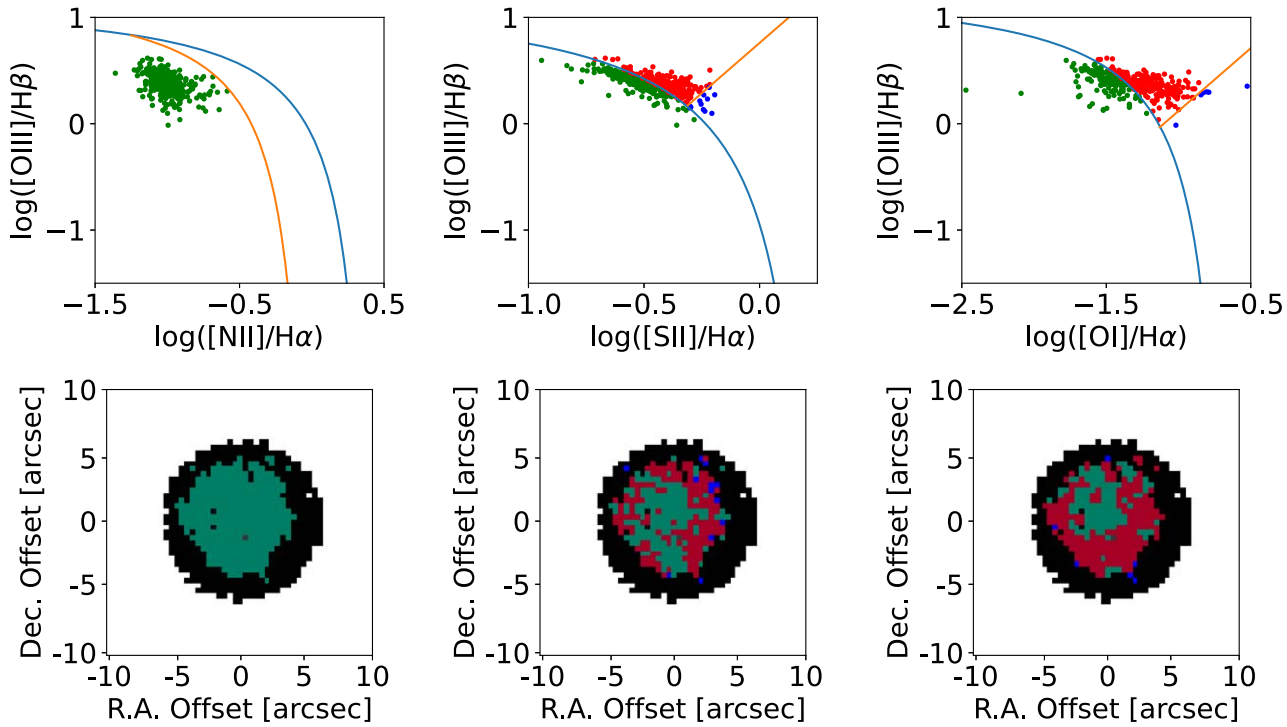

Figure 9. GAMA 273514, which contains AGN-like ionization. The top row shows BPT/VO87 emission-line diagrams and the bottom row presents spatial maps colored according to the diagnostic directly above it. There is no clear pattern in any of the spatial maps that suggests true ionization from a central AGN, despite the emission-line diagnostics having a large number of AGN-like spaxels.

shocks within a single galaxy, only the ionization source detected will have a nonzero map. The amount of ionization is determined by weighting a spaxel's distance along the mixing sequence starting at the base of the star-forming track by the flux in Hα for each component and summing the totals together. The mixing sequence is created by plotting a best-fit line of the points that lie above the velocity dispersion threshold in 3D space from the lowest to highest values in velocity dispersion. This effectively traces the path from the base of the star formation sequence up into the high-velocity-dispersion, non-star-forming regions. For the galaxies that host unidentified non-star-forming ionization, we list their non-star-forming component as negative values in both the AGN and shock maps to denote the uncertainty in what the major driver of this ionization is. Examples of three galaxies with shock, AGN, and elevated velocity dispersion, low emission-line ionization are shown in Figure 12. Along with these ionization maps, we will release a catalog denoting which sources of ionization are detected in each galaxy. These data products will be released for public use alongside other SAMI Galaxy Survey value-added products through the data central database[11].

[11] https://datacentral.org.au/

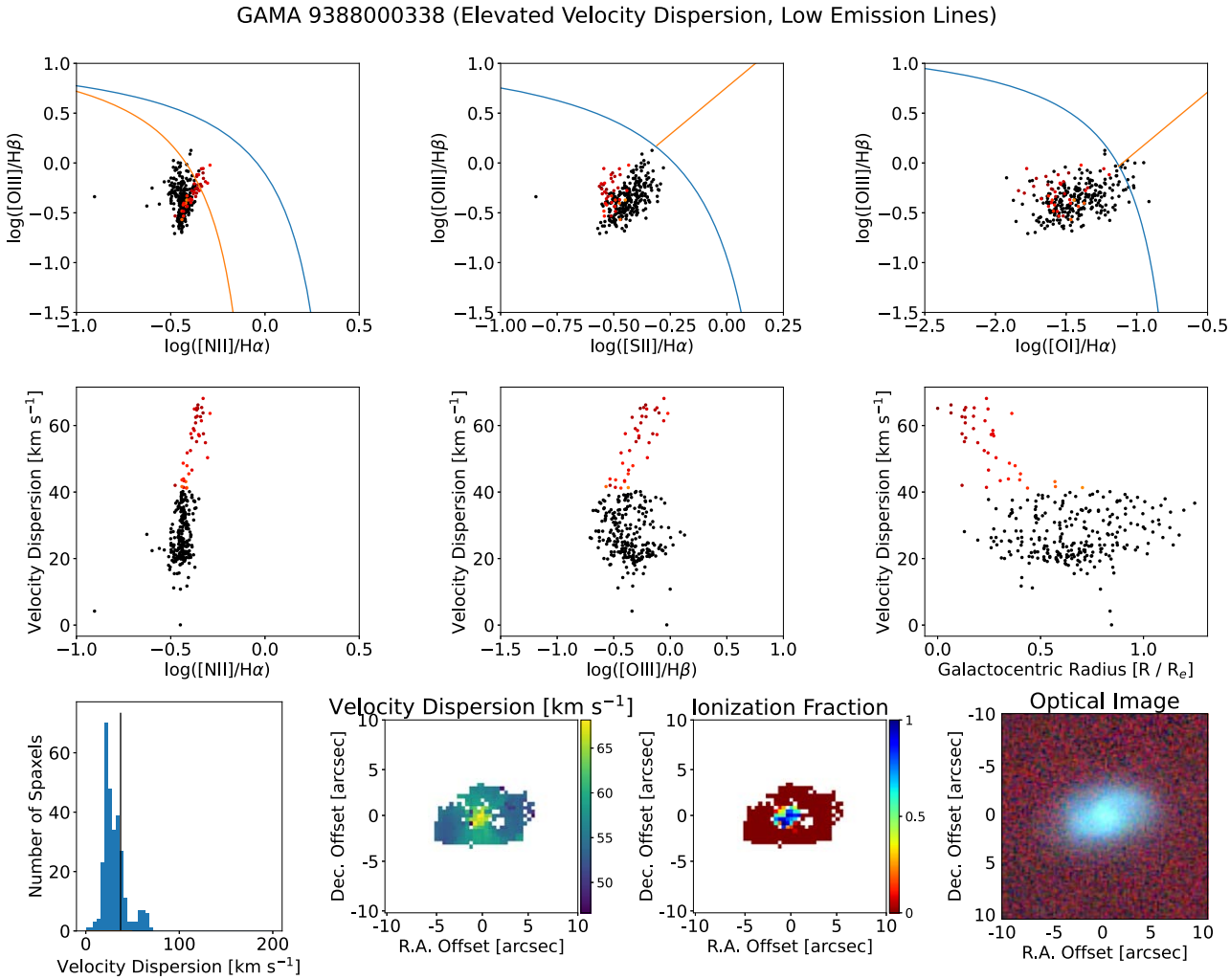

Figure 10. Emission-line diagnostics and maps for GAMA 9388000338, a galaxy containing elevated velocity dispersion, low emission-line spaxels. Each figure in the first row shows the emission-line diagnostics colored according to where each spaxel falls in its respective diagram: green for star-forming, blue for composite or LINER, and red for AGN. Below each diagnostic is the corresponding spatial map showing where in the galaxy the points in the diagram above are located. The middle row contains plots of log([N II]/Hα), log([O III]/Hβ), and effective radius vs. velocity dispersion with points being colored black if they lie below the velocity dispersion cutoff, and colored by increasing radius if they lie above it. The last row contains a histogram of the velocity dispersion with a vertical line denoting the two components in velocity dispersion space, a map of the velocity dispersion in the middle, a map of the ionization fraction tracing the elevated velocity dispersion from lowest to highest values, and a three-color image on the right matching the FOV of the SAMI data.

7. Conclusion

We have investigated a new way of classifying the excitation sources of warm ionized gas in a galaxy using a new multidimensional diagnostic diagram. Our classification method takes advantage of the multiple levels of data that can be obtained by using IFS. By combining emission-line ratios, gas kinematics, and spatial information, we determine the primary excitation source for individual spaxels of a galaxy. Our new method was tested using the SAMI Galaxy Survey, but is general enough to be used with any IFS data set.

Out of the 1996 galaxies used in our sample, our new method finds 409 galaxies with gas ionized by shocks, and 138 galaxies with gas ionized by a central AGN as compared to 233 and 88 respectively using emission-line diagnostics alone. We also identify and label sources of ionization not accounted for in standard emission-line diagnostics such as from diffuse ionized gas and hot, low-mass evolved stars. The combination of gas kinematics and emission-line ratios enables better detection of low powered, non-star-forming ionization sources. Coupled together with spatial information on a per-spaxel basis, we are able to determine a star-forming to AGN or shock mixing sequence for those galaxies that are not dominated by pure star formation.

We also classify a total of 356 galaxies as hosting a spatially incoherent ionization of both high emission-line ratios and low velocity dispersions not typically associated with either pure star formation, AGNs, or shock ionization. Of these, 105 galaxies show LINER-like emission and 251 show AGN-like emission, which we label as diffuse ionized gas and AGN-like respectively. We find an additional 173 galaxies that show increased emission-line ratios and kinematics, but low $EW_{H\alpha}$ consistent with ionization from hot low-mass evolved stars. Finally, we find 357 galaxies containing non-star-forming-like velocity dispersions that we are unable to distinguish between low-luminosity AGNs, shocks, and beam-smearing. These galaxies are characterized as containing elevated kinematics and low emission-line ratios.

In addition to the results presented in this paper, we will be releasing shock maps for all of the galaxies contained within SAMI DR3. These data products will show the fractional

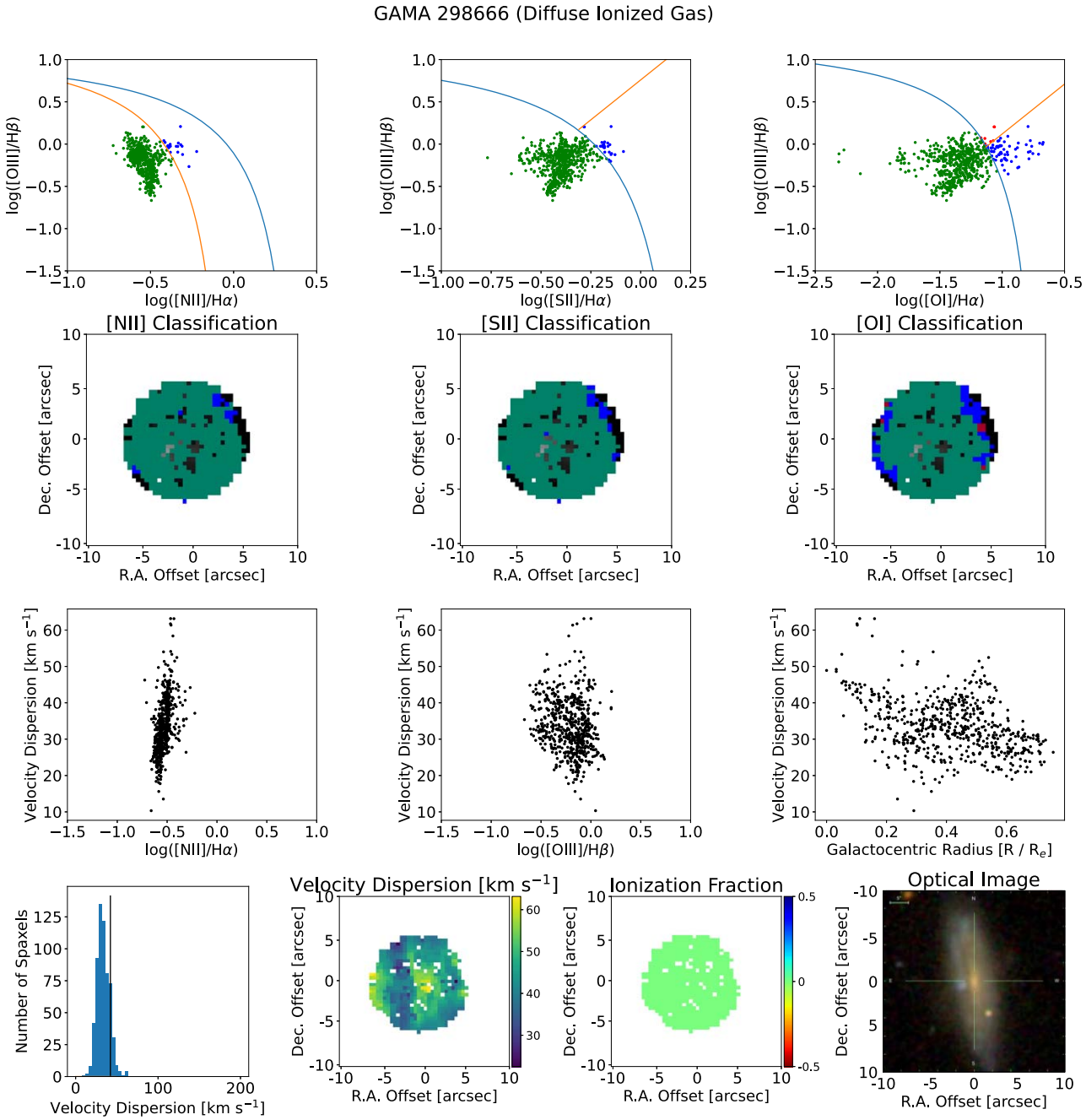

Figure 11. Emission-line diagnostics and maps for GAMA 298666, a galaxy containing diffuse ionized gas. Each panel in the first row shows the emission-line diagnostics colored according to where each spaxel falls in its respective diagram: green for star-forming, blue for composite or LINER, and red for AGN. Below each diagnostic is the corresponding spatial map showing where in the galaxy the points in the diagram above are located. The middle row contains plots of log([N II]/Hα), log([O III]/Hβ), and effective radius vs. velocity dispersion. As our method classifies all of the spaxels as being dominated by star formation, all of the points here are labeled black. The last row contains a histogram of the velocity dispersion with a vertical line denoting the two components in velocity dispersion space, a map of the velocity dispersion in the middle, a spatial map showing that there is no ionization contribution from non-star-forming sources, and a three-color image on the right matching the FOV of the SAMI data.

contribution of ionization on a per-spaxel basis as well as the associated ionization source. The finalized shock maps will be available to download through https://datacentral.org.au/.

Acknowledgments

The authors wish to pay respect to the Gamilaraay/Kamilaroi language group Elders—past, present, and future—of the traditional lands on which the Siding Spring Observatory stands. V.D.J. and A.M.M. acknowledge support from the National Science Foundation under grant No. 2009416. J.v.d.S. acknowledges support of an Australian Research Council Discovery Early Career Research Award (project number DE200100461) funded by the Australian Government. Parts of this research were supported by the Australian Research Council Centre of Excellence for All Sky Astrophysics in 3 Dimensions (ASTRO 3D), through project number CE170100013. The SAMI Galaxy Survey is based on observations made at the Anglo-Australian Telescope. The Sydney-AAO Multi-object Integral field spectrograph (SAMI) was developed jointly by the University

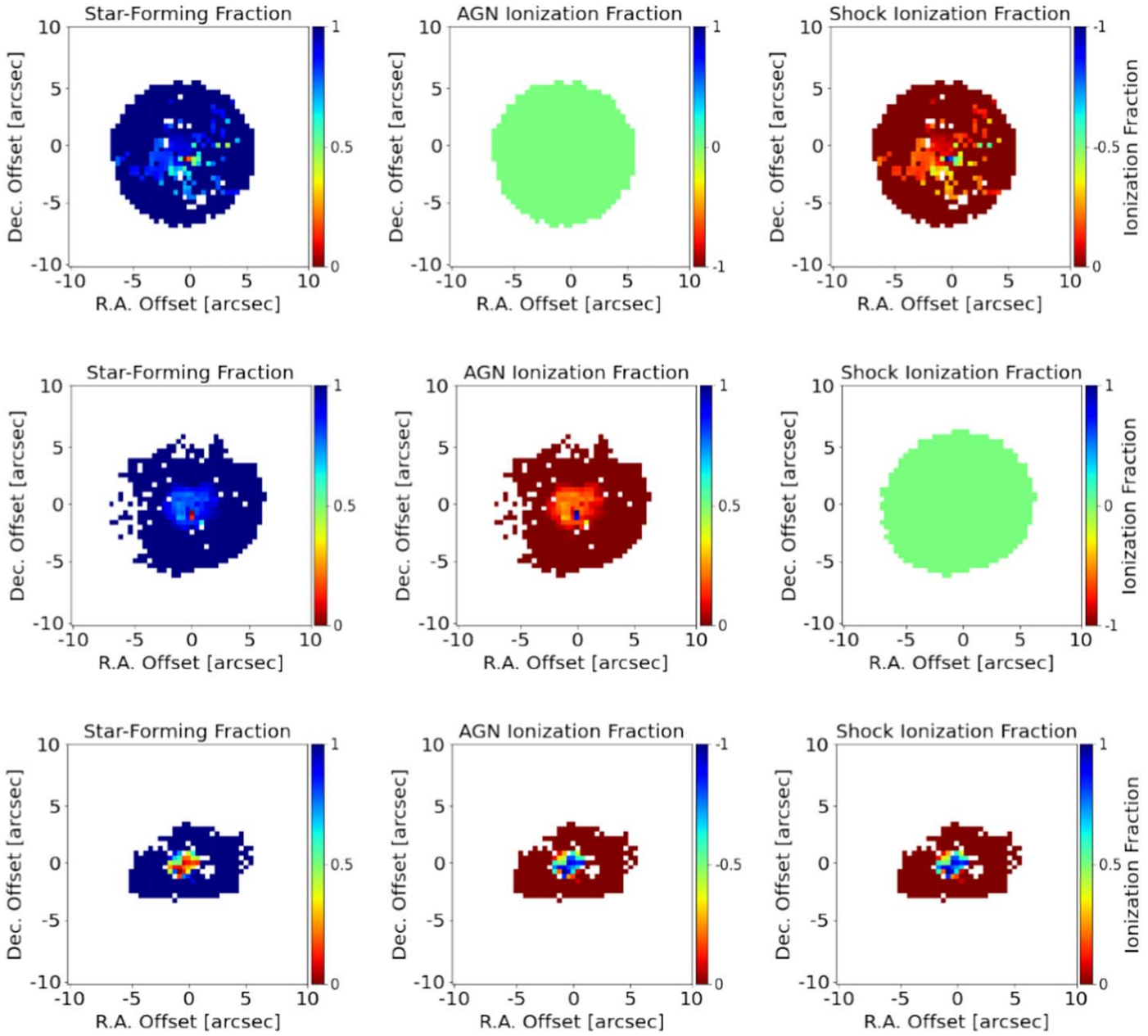

Figure 12. Examples of ionization maps for GAMA 106717, 376478, and 9388000338 (left to right). The relative contribution of each driving power source is shown as a fraction of the total amount of ionization. For galaxies with either AGN- or shock-driven ionization, the corresponding layers are mapped according to the mixing sequence identified by our method. As our method cannot separate ionization sources within a single galaxy, one layer will have no contribution to the total ionization. For galaxies where non-star-forming ionization is detected but we cannot definitively determine between shocks, AGNs, and beam-smearing, a map of negative values is placed in both layers to denote this uncertainty.

of Sydney and the Australian Astronomical Observatory. The SAMI input catalog is based on data taken from the Sloan Digital Sky Survey, the GAMA Survey and the VST ATLAS Survey. The SAMI Galaxy Survey is supported by the Australian Research Council Centre of Excellence for All Sky Astrophysics in 3 Dimensions (ASTRO 3D), through project number CE170100013, the Australian Research Council Centre of Excellence for All-sky Astrophysics (CAASTRO), through project number CE110001020, and other participating institutions. The SAMI Galaxy Survey website is http://sami-survey.org/.

This paper includes data that have been provided by AAO Data Central (datacentral.org.au).

Appendix
3D Diagrams

Figures 13, 14, and 15 are three-dimensional diagnostic diagrams for each of the galaxies discussed in this paper. Interactive versions of these figures can be found in the online version of this journal.

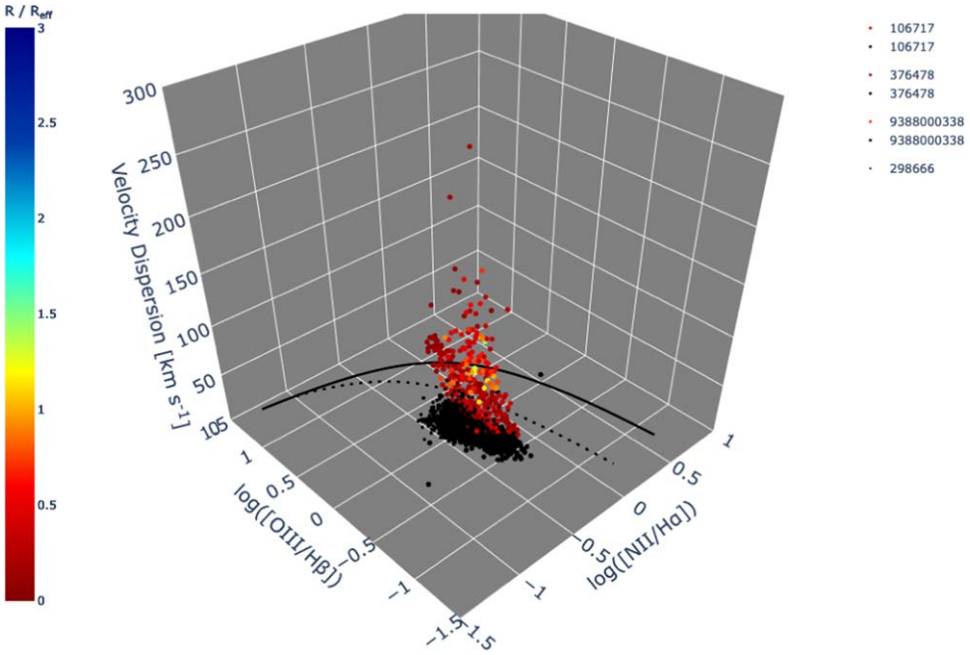

Figure 13. A three-dimensional view of our new emission-line diagnostic using the log([N II]/Hα) emission-line pair for GAMA 106717, 376478, 9388000338, and 298666. The online interactive figure allows for the plot to be rotated, zoomed in and out, and for each galaxy to be turned on and off in the figure by selecting it from the legend. (An interactive version of this figure is available online.)

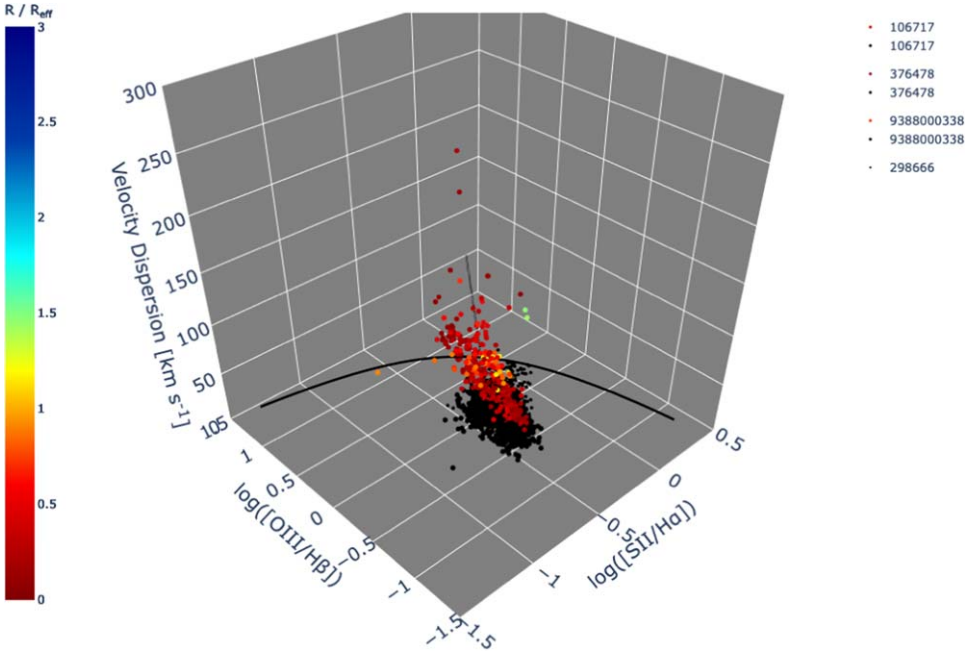

Figure 14. A three-dimensional view of our new emission-line diagnostic using the log([S II]/Hα) emission-line pair for GAMA 106717, 376478, 9388000338, and 298666. The online interactive figure allows for the plot to be rotated, zoomed in and out, and for each galaxy to be turned on and off in the figure by selecting it from the legend. (An interactive version of this figure is available online.)

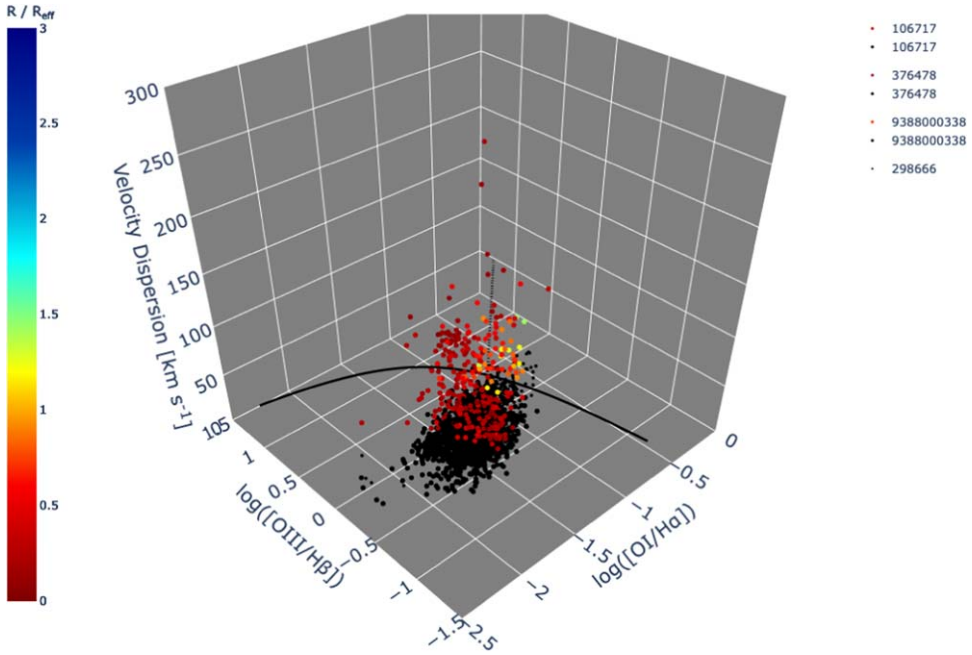

Figure 15. A three-dimensional view of our new emission-line diagnostic using the log([O I]/Hα) emission-line pair for GAMA 106717, 376478, 9388000338, and 298666. The online interactive figure allows for the plot to be rotated, zoomed in and out, and for each galaxy to be turned on and off in the figure by selecting it from the legend. (An interactive version of this figure is available online.)

ORCID iDs

Anne M. Medling https://orcid.org/0000-0001-7421-2944
Brent Groves https://orcid.org/0000-0002-9768-0246
Lisa J. Kewley https://orcid.org/0000-0001-8152-3943
Luca Cortese https://orcid.org/0000-0002-7422-9823
Scott Croom https://orcid.org/0000-0003-2880-9197
Ángel R. López-Sánchez https://orcid.org/0000-0001-8083-8046
Henry Zovaro https://orcid.org/0000-0003-4334-9811
Joss Bland-Hawthorn https://orcid.org/0000-0001-7516-4016
Julia Bryant https://orcid.org/0000-0003-1627-9301
Jon Lawrence https://orcid.org/0000-0002-6998-6993
Matt Owers https://orcid.org/0000-0002-2879-1663
Samuel Richards https://orcid.org/0000-0002-5368-0068
Jesse van de Sande https://orcid.org/0000-0003-2552-0021

References

Abdurro'uf, Accetta, K., Aerts, C., et al. 2022, ApJS, 259, 35
Adelman-McCarthy, J. K., Agüeros, M. A., Allam, S. S., et al. 2006, ApJS, 162, 38
Allen, M. G., Groves, B. A., Dopita, M. A., Sutherland, R. S., & Kewley, L. J. 2008, ApJS, 178, 20
Baldwin, J. A., Phillips, M. M., & Terlevich, R. 1981, PASP, 93, 5
Belfiore, F., Santoro, F., Groves, B., et al. 2022, A&A, 659, A26
Binette, L., Magris, C. G., Stasińska, G., & Bruzual, A. G. 1994, A&A, 292, 13
Bland-Hawthorn, J., Bryant, J., Robertson, G., et al. 2011, OExpr, 19, 2649
Bryant, J. J., Bland-Hawthorn, J., Fogarty, L. M. R., Lawrence, J. S., & Croom, S. M. 2014, MNRAS, 438, 869
Bryant, J. J., Owers, M. S., Robotham, A. S. G., et al. 2015, MNRAS, 447, 2857
Cid Fernandes, R., Stasińska, G., Mateus, A., & Vale Asari, N. 2011, MNRAS, 413, 1687
Cid Fernandes, R., Stasińska, G., Schlickmann, M. S., et al. 2010a, MNRAS, 403, 1036
Cid Fernandes, R., Stasińska, G., Vale Asari, N., et al. 2010b, in IAU Symp. 267, Co-Evolution of Central Black Holes and Galaxies, ed. B. M. Peterson, R. S. Somerville, & T. Storchi-Bergmann (Cambridge: Cambridge Univ. Press), 65
Croom, S. M., Lawrence, J. S., Bland-Hawthorn, J., et al. 2012, MNRAS, 421, 872
Croom, S. M., Owers, M. S., Scott, N., et al. 2021, MNRAS, 505, 991
D'Agostino, J. J., Kewley, L. J., Groves, B. A., et al. 2019, MNRAS, 487, 4153
D'Agostino, J. J., Poetrodjojo, H., Ho, I. T., et al. 2018, MNRAS, 479, 4907
Davies, R. L., Kewley, L. J., Ho, I. T., & Dopita, M. A. 2014a, MNRAS, 444, 3961
Davies, R. L., Rich, J. A., Kewley, L. J., & Dopita, M. A. 2014b, MNRAS, 439, 3835
Dove, J. B., & Shull, J. M. 1994, ApJ, 430, 222
Driver, S. P., Hill, D. T., Kelvin, L. S., et al. 2011, MNRAS, 413, 971
Groves, B. A., Heckman, T. M., & Kauffmann, G. 2006, MNRAS, 371, 1559
Hainline, K. N., Hickox, R. C., Greene, J. E., et al. 2014, ApJ, 787, 65
Hampton, E. J., Medling, A. M., Groves, B., et al. 2017, MNRAS, 470, 3395
Ho, I. T., Kewley, L. J., Dopita, M. A., et al. 2014, MNRAS, 444, 3894
Ho, I. T., Medling, A. M., Groves, B., et al. 2016, Ap&SS, 361, 280
Husemann, B., Jahnke, K., Sánchez, S. F., et al. 2014, MNRAS, 443, 755
Kauffmann, G., Heckman, T. M., Tremonti, C., et al. 2003, MNRAS, 346, 1055
Kewley, L. J., Dopita, M. A., Sutherland, R. S., Heisler, C. A., & Trevena, J. 2001, ApJ, 556, 121
Kewley, L. J., Groves, B., Kauffmann, G., & Heckman, T. 2006, MNRAS, 372, 961
Kewley, L. J., Nicholls, D. C., & Sutherland, R. S. 2019, ARA&A, 57, 511
Lacerda, E. A. D., Cid Fernandes, R., Couto, G. S., et al. 2018, MNRAS, 474, 3727
Lacerda, E. A. D., Sánchez, S. F., Cid Fernandes, R., et al. 2020, MNRAS, 492, 3073
Law, D. R., Belfiore, F., Bershady, M. A., et al. 2022, ApJ, 928, 58
Law, D. R., Ji, X., Belfiore, F., et al. 2021, ApJ, 915, 35
López-Cobá, C., Sánchez, S. F., Anderson, J. P., et al. 2020, AJ, 159, 167
López-Cobá, C., Sánchez, S. F., Bland-Hawthorn, J., et al. 2019, MNRAS, 482, 4032
McElroy, R., Croom, S. M., Pracy, M., et al. 2015, MNRAS, 446, 2186
Medling, A. M., U, V., Rich, J. A., et al. 2015, MNRAS, 448, 2301
Medling, A. M., Cortese, L., Croom, S. M., et al. 2018, MNRAS, 475, 5194
Micheva, G., Roth, M. M., Weilbacher, P. M., et al. 2022, A&A, 668, A74
Miller, S. T., & Veilleux, S. 2003, ApJ, 592, 79
Monreal-Ibero, A., Arribas, S., & Colina, L. 2006, ApJ, 637, 138
Monreal-Ibero, A., Arribas, S., Colina, L., et al. 2010, A&A, 517, A28
Owers, M. S., Allen, J. T., Baldry, I., et al. 2017, MNRAS, 468, 1824

Reynolds, R. J., Scherb, F., & Roesler, F. L. 1973, ApJ, 185, 869
Rich, J. A., Kewley, L. J., & Dopita, M. A. 2011, ApJ, 734, 87
Rich, J. A., Kewley, L. J., & Dopita, M. A. 2014, ApJL, 781, L12
Rich, J. A., Kewley, L. J., & Dopita, M. A. 2015, ApJS, 221, 28
Rodríguez del Pino, B., Arribas, S., Piqueras López, J., Villar-Martín, M., & Colina, L. 2019, MNRAS, 486, 344
Sánchez, S. F. 2020, ARA&A, 58, 99
Sánchez, S. F., Avila-Reese, V., Hernandez-Toledo, H., et al. 2018, RMxAA, 54, 217
Sánchez, S. F., García-Benito, R., Zibetti, S., et al. 2016, A&A, 594, A36
Sánchez, S. F., Pérez, E., Rosales-Ortega, F. F., et al. 2015, A&A, 574, A47
Sánchez, S. F., Walcher, C. J., Lopez-Cobá, C., et al. 2021, RMxAA, 57, 3
Scott, N., van de Sande, J., Croom, S. M., et al. 2018, MNRAS, 481, 2299
Sharp, R. G., & Bland-Hawthorn, J. 2010, ApJ, 711, 818
Stasińska, G., Vale Asari, N., Cid Fernandes, R., et al. 2008, MNRAS, 391, L29
Thomas, A. D., Dopita, M. A., Shastri, P., et al. 2017, ApJS, 232, 11
Thomas, A. D., Groves, B. A., Sutherland, R. S., et al. 2016, ApJ, 833, 266
van de Sande, J., Bland-Hawthorn, J., Fogarty, L. M. R., et al. 2017, ApJ, 835, 104
Veilleux, S., & Osterbrock, D. E. 1987, ApJS, 63, 295
Wake, D. A., Bundy, K., Diamond-Stanic, A. M., et al. 2017, AJ, 154, 86